PAPER

Check for updates

Use of real-time *in situ* monitoring as a tool for comparing electrochemical advanced oxidation processes for the decolourisation of triarylmethane dyes

Chelsea M. Schroeder, [ID] Lucas W. Denucci and Nicholas E. Leadbeater [ID] *

This study explores a phosphate-based electrochemical advanced oxidation process (EAOP) for the decolourisation of synthetic dyes in wastewater. A real-time *in situ* UV-Vis spectrophotometric system enabled continuous monitoring of dye decolourisation, allowing for high-throughput optimisation of reaction conditions using phenol red as a model compound. The optimised system demonstrated superior performance compared to anodic oxidation and electrochemically activated persulphate systems. Further analysis of six triarylmethane dyes revealed that structural features, such as substitution near the central carbon and halogenation, significantly impact decolourisation efficiency. Among the dyes studied, bromocresol purple exhibited the fastest decolourisation, reaching 99% colour removal in 19 min, while tetrabromophenol blue was the slowest, requiring 34 min to reach a similar level of decolourisation. Overall, this system offers an effective, pH-stable, and environmentally conscious alternative for wastewater remediation.

Introduction

Projections suggest that over 40% of the global population will not have adequate access to clean drinking water by 2030.[1,2] Among the contributing factors, pollution from textile dyes is of particular concern, with an estimated 280 000 tons of synthetic dyes released into the environment annually.[3] These dyes, characterised by their extensive conjugation, are intensely coloured, toxic, and chemically persistent, making them resistant to conventional water treatment methods. In response to this challenge, electrochemical advanced oxidation processes (EAOPs) have emerged as promising technology for dye degradation due to their efficiency, small operational footprint, limited chemical consumption, and ease of automation. EAOPs operate by generating highly reactive radical species *in situ*. These radicals oxidise and degrade complex pollutants into smaller intermediates, with the potential for complete mineralisation to carbon dioxide and water.[4–6]

The efficiency of electrochemical advanced oxidation processes (EAOPs) is strongly influenced by the type of anode employed and the radical species it generates. Active anodes, such as graphite or platinum, are constrained by their low oxygen evolution potentials (OEP), typically facilitating pollutant degradation through hydroxyl radical formation (2.8 V *vs.* SHE) or *via* direct electron transfer at the anode surface;

a process known as anodic oxidation (AO). As a surface-confined process, AO can be enhanced through the use of inactive anodes such as boron doped diamond (BDD) or lead(IV) oxide. These materials possess significantly higher OEPs, enabling the generation of highly oxidising radical species from supporting electrolytes, such as sulphates, chlorides, or phosphates, within the bulk solution.[1,5,7–9] Sulphate-based EAOPs, including electrochemically activated persulphate (EAP) (Fig. 1), have been extensively investigated.[6,8,10] In contrast, phosphate-based systems, remain comparatively underexplored.[11]

Phosphate radicals can exist in three forms ($H_2PO_4^{\bullet}$, $HPO_4^{\bullet-}$, and $PO_4^{\bullet 2-}$) depending on the pH of the solution. Dihydrogen phosphate, the primary radical at pH 7, has the highest oxidation potential at 2.75 V *vs.* SHE. This radical displays reactivity and selectivity comparable to that of the sulphate radical, with both species favoring hydrogen atom abstraction mechanisms and displaying similar rates of reaction with aliphatic and aromatic carboxylic acids. While the influence of phosphate species on sulphate-based EAOPs has been frequently examined due to the prevalence of phosphates in textile effluent, the inverse scenario has received significantly less attention in the literature.[11–16]

A major challenge hindering the widespread implementation of EAOPs in water treatment is the lack of methodological uniformity. Many EAOPs are developed for the degradation of a single model pollutant, leaving their performance on structurally diverse compounds uncertain. This variability complicates efforts to systematically assess the impact of pollutant

Department of Chemistry, University of Connecticut, 55 North Eagleville Road, Storrs, Connecticut 06269, USA. E-mail: nicholas.leadbeater@uconn.edu
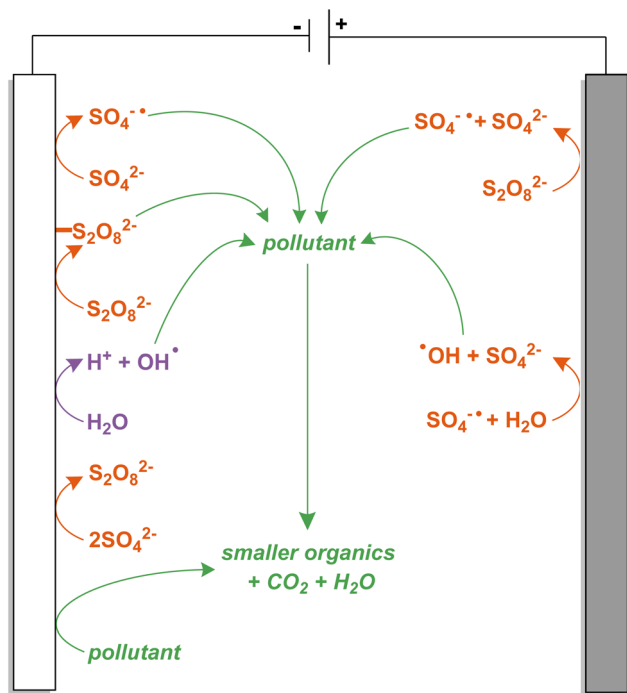
Fig. 1 Electrochemically activated persulphate.

structure on degradation efficiency.[3,8,17] To overcome this limitation, our research group developed a real-time *in situ* continuous monitoring apparatus that enables facile screening of EAOPs using UV-visible (UV-Vis) spectrophotometry (Fig. 2). The apparatus includes a 3D-printed vial holder that minimises external light interference, a precision-aligned LED light source, and an optical fiber connected to a UV-vis spectrophotometer. This configuration enables the collection of absorbance
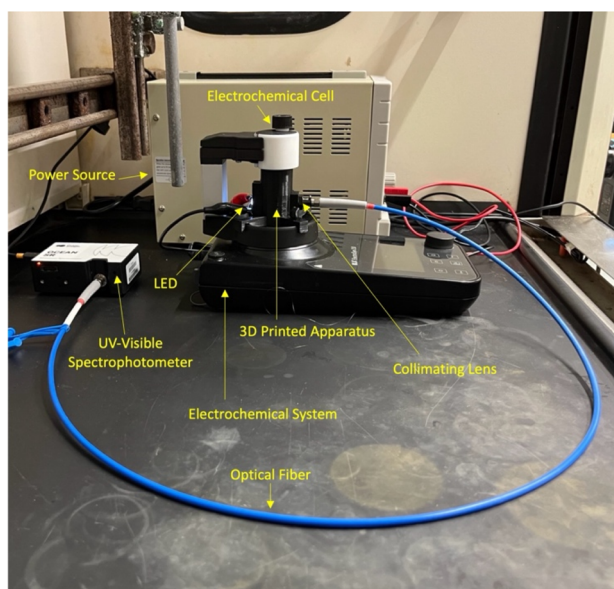

Fig. 2 Real-time *in situ* continuous monitoring apparatus (48 × 61 × 20 cm).

measurements without the need for sample manipulation, substantially accelerating data acquisition. Real-time monitoring is essential, as delayed sampling can lead to artificially inflated decolourisation values.[18–20] While comparable systems include external flow-through cuvettes[21] or HPLC monitoring arrangements,[22] our design offers the unique advantage of real-time *in situ* monitoring, ensuring accurate and representative data on dye decolourisation kinetics.

In this study, we utilised our continuous monitoring apparatus to develop an electrochemically activated phosphate buffer (EAPB) system operating at neutral pH. The performance of the EAPB system was systematically evaluated against previously developed electrochemically activated persulphate (EAP)[19] and anodic oxidation (AO)[18] systems. To investigate the influence of dye structure and oxidant identity on the speed of decolourisation, we examined six structurally related, pH-sensitive triarylmethane dyes across all three systems (EAPB, EAP, and AO).

Results and discussion

Optimisation of electrochemically activated phosphate buffer decolourisation

As an initial step in this study, we investigated phosphate-mediated decolourisation using phenol red (PR) as a model substrate. Initial conditions were established as 100 μM PR in phosphate buffer (100 mM, pH 7, 8 mL), graphite electrodes, an applied current of 5 mA, and stirring at 1000 rpm. These parameters served as a baseline for systematically evaluating the effects of electrode composition, current density, buffer concentration, and the addition of supplemental electrolytes on the rate of decolourisation.

Boron-doped diamond (BDD) anodes are widely regarded as more effective than graphite anodes in EAOPs.[1] To validate this, we evaluated three electrode pairings using commercially available graphite and BDD electrodes. Decolourisation reactions were monitored over time, with results plotted as the percentage of dye remaining. As shown in Fig. 3, the system employing two graphite electrodes exhibited the slowest
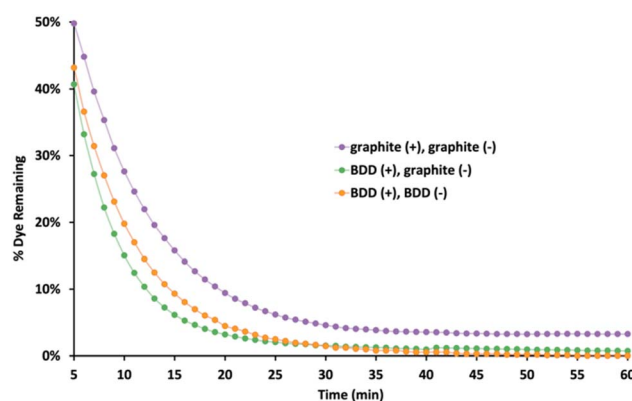

Fig. 3 Effect of electrode configuration on the decolourisation of PR. Conditions: [PR] = 100 μM, 100 mM pH 7 phosphate buffer, I = 5 mA, stirring = 1000 rpm.

decolourisation, whereas the combination of a BDD anode and a graphite cathode achieved the highest efficiency. These results indicate that optimal performance can be achieved without using two BDD electrodes, offering a more cost-effective alternative without compromising efficiency.[19]

Next, the effect of applied current on the rate of decolourisation was investigated. Fig. 4 presents the first order rate constants measured at 10 min for applied currents of 0, 5, 10, and 15 mA. As anticipated for an electrochemical process, no decolourisation occurred in the absence of applied current. The rate constant increased from 3.16×10^{-3} s^{-1} at 5 mA to a maximum of 3.56×10^{-3} s^{-1} at 10 mA, followed by a notable decrease to 2.99×10^{-3} s^{-1} at 15 mA. Although increasing current generally enhances the decolourisation rate, elevated currents also promote competing side reactions, such as oxygen and hydrogen evolution, which reduce the efficiency of the desired oxidation process.[8,23]

To minimise chemical consumption, the effect of buffer concentration on the decolourisation process was evaluated to determine the lowest concentration that maintains pH stability. The first order rate constants for 100, 50, and 10 mM pH 7 phosphate buffers were nearly identical at 10 min, measured at 3.56×10^{-3} s^{-1}, 3.66×10^{-3} s^{-1}, and 3.64×10^{-3} s^{-1}, respectively (Fig. 5). A lower buffer concentration of 1 mM was also tested; however, data acquisition was not possible due to the reaction voltage reaching the safety limit of the electrochemistry apparatus. Under these conditions, the speed of decolourisation appears independent of the buffer concentration, provided sufficient buffer is present to serve as the electrolyte. The pH of each reaction was measured every 15 min, and the results can be seen in Fig. 6. The 100 mM reaction stayed very close to pH 7 for its entirety, lowering only slightly to 6.97 after 1 h. Lower buffer concentrations exhibited less pH control, with the 50 mM and 10 mM buffers decreasing to pH values of 6.83 and 6.74, respectively, after 1 h. Balancing pH stability and atom economy, the 50 mM buffer was selected as the optimal concentration for subsequent experiments.
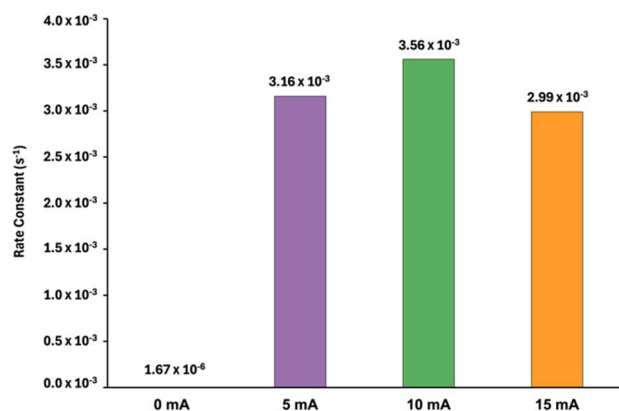

Fig. 5 Effect of varying the concentration of phosphate buffer on the first order rate constants at 10 min. Conditions: [PR] = 100 µM, BDD anode, graphite cathode, I = 10 mA, stirring = 1000 rpm.

Sodium persulphate and sodium chloride are common additives in EAOPs due to their capacity to generate highly oxidising radical species under electrochemical conditions. The presence of persulfate can lead to the formation of sulphate radicals (SO$_4$$^{•-}$, 2.5–3.1 V vs. SHE), while chloride can give rise to chlorine radicals (Cl$^•$, 2.55 V vs. SHE). Of note is that chloride radicals are capable of substitution reactions on aromatic rings, contributing to both decolourisation and possible halogenation pathways. In contrast, sulphate radicals typically engage in hydrogen abstraction and electron transfer rather than substitution.[14] The effect of varying concentrations (7, 14, and 28 mM) of these supplemental electrolytes on the rate of decolourisation was investigated (Fig. 7). Concentrations below 7 mM were not tested due to limitations in solution preparation. The addition of 7 mM sodium persulphate had a negligible effect on the reaction rate. However, increasing sodium persulphate concentrations to 14 and 28 mM resulted in a progressive decline in the rate constant from 3.66×10^{-3} s^{-1} without additive to 3.41×10^{-3} s^{-1} and 2.85×10^{-3} s^{-1}, respectively. This reduction in efficiency is attributed to enhanced radical–radical termination reactions at higher persulphate

Fig. 4 Effect of varying applied current on the first order rate constants at 10 min for the decolourisation of PR. Conditions: [PR] = 100 µM, BDD anode, graphite cathode, 100 mM pH 7 phosphate buffer, stirring = 1000 rpm.
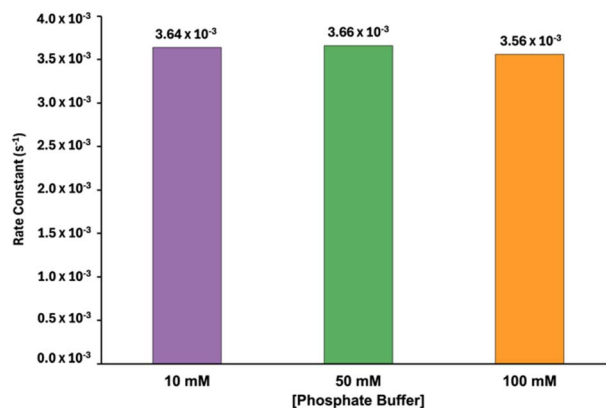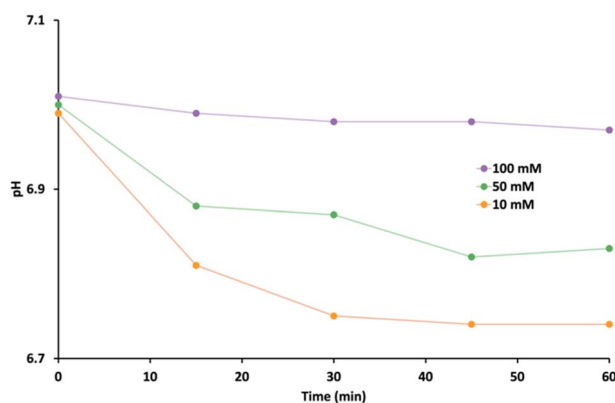

Fig. 6 Change in pH over time for reactions with varying phosphate buffer concentrations. Conditions: [PR] = 100 µM, BDD anode, graphite cathode, I = 10 mA, stirring = 1000 rpm.
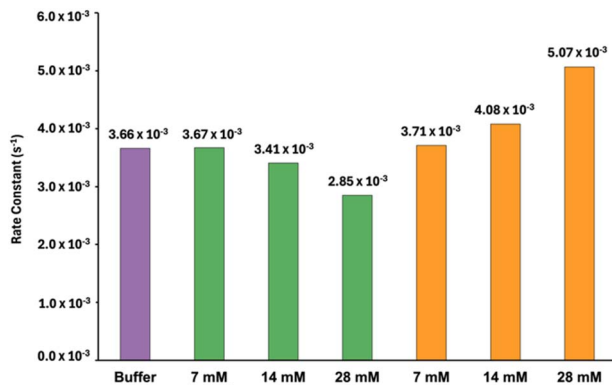
Fig. 7 Effect of supplemental electrolytes on the first order rate constants at 10 min. Conditions: [PR] = 100 μM, BDD anode, graphite cathode, 50 mM pH 7 phosphate buffer, I = 10 mA, stirring = 1000 rpm.

Fig. 9 Absorbance spectrum of PR decolourisation from 3–45 min. Conditions: [PR] = 100 μM, BDD anode, graphite cathode, 50 mM pH 7 phosphate buffer, I = 10 mA, stirring = 1000 rpm.

concentrations, which decrease the availability of reactive oxidising species for pollutant decolourisation.[23]

At first glance, the addition of sodium chloride appears beneficial, as the first order rate constants increase exponentially with increasing sodium chloride concentration. However, rate constants derived from a single λ_{max} value do not capture the full complexity of the system. Fig. 8 presents the UV-Vis spectra reordered over the course of a reaction containing 28 mM sodium chloride, while Fig. 9 shows the corresponding spectra for a reaction without added electrolyte. In the presence of sodium chloride, the λ_{max} of phenol red (434 nm) decreased rapidly and was replaced by a new absorption band between 560–580 nm. This shift is consistent with the potential formation of chlorinated byproducts such as chlorophenol red, which has a reported λ_{max} value of 572 nm at pH 6.7. The most likely pathway involves anodic oxidation of chloride ions to chlorine radicals or free chlorine species which subsequently undergo electrophilic substitution on the aromatic ring of phenol red. These results indicate that the use of chloride-containing electrolytes in EAOPs can promote the formation of chlorinated
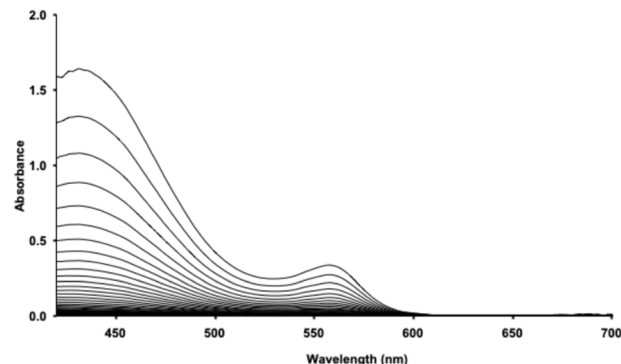
intermediates, which are often more environmentally persistent than their non-chlorinated counterparts.[1,21] Well-documented examples of persistent chlorinated species include polychlorinated biphenyls (PCBs) and dichlorodiphenyltrichloroethane (DDT). Chlorinated compounds are well known to be toxic due to their ability to induce oxidative stress in biological systems.[2] While many reported EAOPs have concluded that the inclusion of chlorine radicals as oxidizing species can justify the associated risks,[1] our data suggest otherwise for this system. Based on these findings, we elected to exclude sodium chloride from subsequent experiments to avoid the formation of potentially persistent and toxic chlorinated intermediates.

Effects of varying dye structure on decolourisation efficiency

With optimised conditions of 100 μM dye in phosphate buffer (50 mM, pH 7, 8 mL), BDD anode, graphite cathode, applied current (10 mA), with stirring (1000 rpm) in hand, we transitioned to determining how varying the pollutant structure impacts the rate of decolourisation. For this comparison, six triarylmethane dyes were selected (Fig. 10). This class of compounds is among the most toxic and mutagenic dyes still
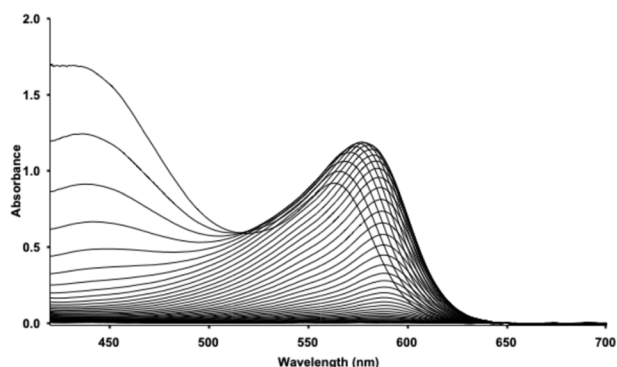

Fig. 8 Absorbance spectrum of PR decolourisation with NaCl as a supplemental electrolyte from 3–45 min. Conditions: [PR] = 100 μM, BDD anode, graphite cathode, 50 mM pH 7 phosphate buffer, [NaCl] = 28 mM, I = 10 mA, stirring = 1000 rpm.
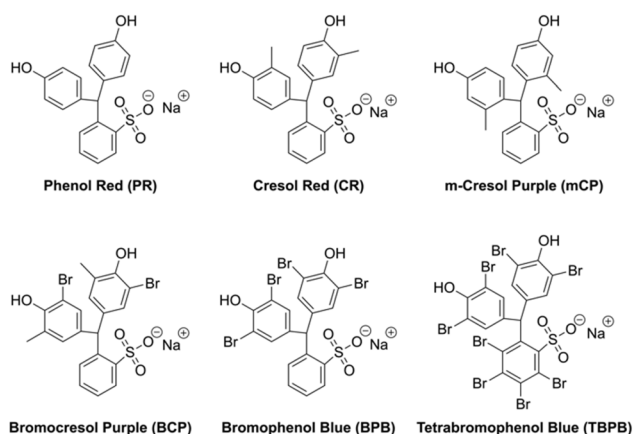

Fig. 10 Structures of triarylmethane dyes compared in this study.

commonly employed in the textile industry due to their wide range of vivid colours. Their toxicity stems from the ability to permeate cell membranes under acidic conditions.[24,25] The dyes examined in this study include Phenol Red (PR), Cresol Red (CR), *m*-Cresol Purple (*m*CP), Bromocresol Purple (BCP), Bromophenol Blue (BPB), and Tetrabromophenol Blue (TBPB).

First order rate constants measured at 20 min are presented in Fig. 11, with additional graphical data available in the SI. Overall, BCP with an EAPB rate of 4.03×10^{-3} s^{-1} was the easiest to decolourise, and TBPB with a rate of 2.35×10^{-3} s^{-1} was the most difficult to remove. All dyes consistently demonstrated faster decolourisation rates under EAPB and EAP conditions compared to AO conditions. This was expected as the EAPB and EAP systems employ BDD anodes, while AO uses graphite electrodes. On average, the EAPB system achieved slightly higher rates of decolourisation than EAP. Considering the similar oxidation potentials and reactivity of phosphate and sulphate radicals, this difference is likely attributable to the pH of the solutions.[11,14] The EAPB system maintains near-neutral pH, where most of the dyes studied exist as a negatively charged or neutral species. In contrast, the EAP system acidifies rapidly, reaching a pH value of 1.96 at 15 min and 1.86 at 1 h. At these acidic pH values, triarylmethane dyes exist exclusively in their cationic forms. Previous studies indicate that cationic pollutants are more resistant to decolourisation than their anionic or neutral counterparts, which may explain the observed variations in rate constants.[19]

PR, CR, and *m*CP differ in the number and position of methyl substituents on the aromatic rings. PR lacks alkyl substituents, CR contains two methyl groups in *ortho* positions relative to the phenol, while *m*CP features two *meta*-methyl groups. Among these, CR exhibited the highest rate of decolourisation (EAPB: 3.27×10^{-3} s^{-1}, EAP: 3.42×10^{-3} s^{-1}, AO: 2.69×10^{-3} s^{-1}), suggesting that electron-donating methyl groups modestly enhance susceptibility to oxidative decolourisation. The pronounced decrease in the rate of decolourisation observed for *m*CP (EAPB: 2.84×10^{-3} s^{-1}, EAP: 2.43×10^{-3} s^{-1}, AO: 9.39×10^{-4} s^{-1}) may arise from increased steric hindrance near the central carbon atom, a key site of attack in a number of the proposed degradation mechanisms for triarylmethane dyes.[26,27]

The influence of halogens on pollutant decolourisation is multifaceted. BCP, BPB, and TBPB differ in both the number and position of bromine substituents: BCP contains two bromine atoms, BPB has four, and TBPB incorporates eight. Among these, BCP exhibited the highest decolourisation rates (EAPB: 4.03×10^{-3} s^{-1}, EAP: 3.64×10^{-3} s^{-1}, AO: 2.67×10^{-3} s^{-1}), suggesting that the presence of a limited number of halogens may enhance decolourisation efficiency.[2,26] However, a progressive increase in halogen content was associated with a substantial decline in decolourisation rates, with TBPB demonstrating the lowest values across all systems (EAPB: 2.35×10^{-3} s^{-1}, EAP: 2.24×10^{-3} s^{-1}, AO: 8.44×10^{-4} s^{-1}). This inverse relationship between halogen content and decolourisation rate is consistent with prior studies on xanthene dyes, such as Acid Red 91 and Acid Red 87, where increasing the number of bromine atoms from two to four reduced the overall reaction rate.[19] The observed resistance to oxidative decolourisation in heavily halogenated compounds may arise from increased steric hindrance at key reactive sites or from the generation of halogen radicals, which can engage in non-productive termination pathways or lead to the formation of more recalcitrant byproducts.

Experimental section

General considerations

An IKA ElectraSyn 2.0 with a standard 10-mL vial was interfaced with an Ocean Insight SR-2UVV400-25 spectrophotometer with a range of 183–909 nm, optical resolution of 1.33 nm, and signal to noise ratio of 380 : 1. The spectrophotometer was attached to an Ocean Insight P400-1-SR 400 nm diameter optical fiber (200 nm–1.1 μm) with a 74-UV collimating lens (185 nm–2.5 μm). A white LED with a range of 420–700 nm was employed as the light source. Data was collected using OceanView 2.0 from Ocean Insight. Graphite and boron doped diamond electrodes, obtained from IKA, were used. The 3D-printed interface (STL file available in the SI) was fabricated from black polylactic acid using an Entina Tina2S 3D-printer.

Chemicals

Cresol red, *m*-cresol purple, bromocresol purple, tetrabromophenol blue, and sodium chloride were obtained from Sigma Aldrich. Phenol red, and bromophenol blue were obtained from Fisher Scientific. Sodium persulphate was obtained from Oakwood Chemical.

General procedure

The 3D-printed sleeve was placed on the stage of the IKA ElectraSyn 2.0 single-vial holder. An optical fiber was attached to the front cavity in the 3D-printed sleeve by means of a collimating lens. The other end of the optical fiber was attached to the spectrophotometer. A standard 5 mm white LED was placed in the slot at the back of the 3D-printed sleeve and connected to a bench power supply using alligator clips. The power supply
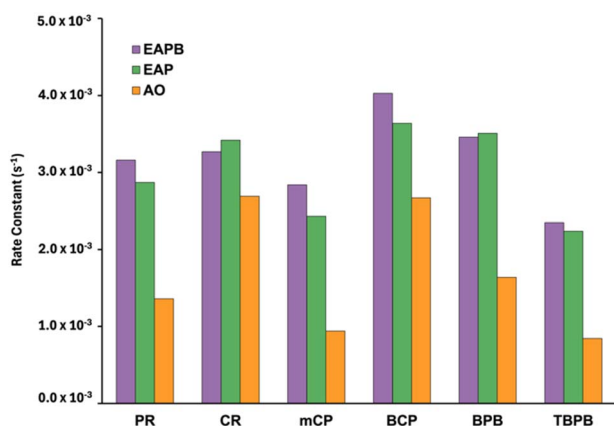

Fig. 11 First order rate constants of six triarylmethane dyes under EAPB, EAP, and AO systems.

was set to 2.6 V and allowed to warm up for 10 min until the absorbance spectrum of the LED remained at a constant intensity. To calibrate the spectrophotometer, a standard 10-mL capacity ElectraSyn 2.0 vial containing deionised water or 50 mM pH 7 phosphate buffer (8 mL) was placed inside of the assembled electrochemical/spectrophotometer interface, and the resulting absorbance spectrum was set to zero.

To prepare a reaction, an ElectraSyn 2.0 vial cap was equipped with the desired anode and cathode. For AO conditions, graphite electrodes were used, while the EAP and EAPB conditions employed a BDD anode and a graphite cathode. For the EAPB system a 10-mL capacity vial was charged with 8 mL of 100 μM dye solution in 50 mM pH 7 phosphate buffer. For the AO and EAP systems 8 mL of a 100 μM dye solution in deionised water was used with solid sodium persulphate (14 mM) added immediately before electrolysis. The reaction vessel was placed inside the assembled electrochemical/spectrophotometer interface, and the contents were electrolysed at a constant current of 10 mA while stirring the reaction mixture at 1000 rpm. Absorbance spectra were collected every minute with an automated clicker until the reaction was deemed complete by *in situ* UV-visible spectrophotometry.

Cartesian points of absorbance *vs.* time at the λ_{max} were transferred to a Google Sheets workbook. All reactions were performed in triplicate, absorbances were averaged and then converted to μM values by employing a calibration curve. Finally, μM values were converted to percent dye remaining and plotted as a function of time. Electrodes were cleaned between trials by rinsing them with water, then acetone, then dried with lab air; additionally the graphite electrodes were polished on 2000 grit sandpaper.

Conclusions

We have performed an evaluation of a phosphate-based electrochemical advanced oxidation process (EAOP) for the decolourisation of synthetic dyes, emphasising the optimisation of operational parameters and the role of pollutant structure in treatment efficiency. Using real-time *in situ* UV-Vis spectrophotometry, we demonstrated that the electrochemically activated phosphate buffer system outperforms both anodic oxidation and electrochemical advanced oxidation. Structure-reactivity analysis of six triarylmethane dyes revealed that both electronic effects and steric hindrance significantly influence decolourisation rates, with dyes bearing minimal substitution near the central carbon and fewer halogens were decolourised more readily, underscoring the importance of molecular architecture in electrochemical advanced oxidation process efficacy. These findings support the viability of phosphate-mediated electrochemical advanced oxidation processes as an effective and sustainable strategy for wastewater treatment and offers valuable insights for the rational design of electrochemical treatment systems based on pollutant characteristics. Further study on the structure of degradation pathways and intermediates formed using LC-MS could augment our findings.

Conflicts of interest

There are no conflicts to declare.

Abbreviations

AO	Anodic oxidation
BCP	Bromocresol purple
BDD	Boron doped diamond
BPB	Bromophenol blue
CR	Cresol red
EAP	Electrochemically activated persulphate
EAPB	Electrochemically activated phosphate buffer
EAOPs	Electrochemical advanced oxidation processes
h	Hours
HPLC	High performance liquid chromatography
I	Current
LED	Light emitting diode
mA	Milliamps
*m*CP	*meta*-Cresol purple
min	Minutes
mM	Millimolar
nm	Nanometers
OEP	Oxygen evolution potential
PR	Phenol red
s	Seconds
SHE	Standard hydrogen electrode
STL	Stereolithography
μM	Micromolar
μm	Micrometer
UV-Vis	UV-visible spectrophotometry
V	Volts
λ_{max}	Lambda max

Data availability

The data supporting this article have been included as part of the SI. See DOI: **https://doi.org/10.1039/d5ra04183j**.

Acknowledgements

Notes and references

1 Y. Bashir, R. Raj, M. M. Ghangrekar, A. K. Nema and S. Das, *RSC Sustainability*, 2023, **1**, 1912–1931.

2 R. Al-Tohamy, S. S. Ali, F. Li, K. M. Okasha, Y. A.-G. Mahmoud, T. Elsamahy, H. Jiao, Y. Fu and J. Sun, *Ecotoxicol. Environ. Saf.*, 2022, **231**, 113160.

3 A. B. Isaev, N. S. Shabanov, A. G. Magomedova, P. V. Nidheesh and M. A. Oturan, *Environ. Chem. Lett.*, 2023, **21**, 2863–2911.

4 A. L. Magdaleno, E. Brillas, S. Garcia-Segura and A. J. Dos Santos, *Sep. Purif. Technol.*, 2024, **345**, 127295.

5 L. D. Paquini, L. T. Marconsini, L. P. R. Profeti, O. S. Campos, D. Profeti and J. Ribeiro, *Braz. J. Chem. Eng.*, 2023, **40**, 623–653.

6 J. Li, Y. Li, Z. Xiong, G. Yao and B. Lai, *Chin. Chem. Lett.*, 2019, **30**, 2139–2146.

7 P. Brosler, A. V. Girão, R. F. Silva, J. Tedim and F. J. Oliveira, *Environments*, 2023, **10**, 15.

8 A. Fernandes, M. J. Nunes, A. S. Rodrigues, M. J. Pacheco, L. Ciríaco and A. Lopes, *Molecules*, 2021, **26**, 4821.

9 Y. Jiang, H. Zhao, J. Liang, L. Yue, T. Li, Y. Luo, Q. Liu, S. Lu, A. M. Asiri, Z. Gong and X. Sun, *Electrochem. Commun.*, 2021, **123**, 106912.

10 L. W. Matzek and K. E. Carter, *Chemosphere*, 2016, **151**, 178–188.

11 Y. Wen, E. Lichtfouse, V. K. Sharma and X. Ma, *Environ. Chem. Lett.*, 2023, **21**, 15–20.

12 G. X. Castillo-Cabrera, C. I. Pliego-Cerdán, E. Méndez and P. J. Espinoza-Montero, *Front. Chem.*, 2024, **11**, 1298630.

13 I. Sirés, E. Brillas, M. A. Oturan, M. A. Rodrigo and M. Panizza, *Environ. Sci. Pollut. Res.*, 2014, **21**, 8336–8367.

14 J. Wang and S. Wang, *Chem. Eng. J.*, 2020, **401**, 126158.

15 E. Weiss, C. Sáez, K. Groenen-Serrano, P. Cañizares, A. Savall and M. A. Rodrigo, *J. Appl. Electrochem.*, 2007, **38**, 93–100.

16 I. M. Sasidharan Pillai and A. K. Gupta, *J. Electroanal. Chem.*, 2016, **762**, 66–72.

17 C. K. C. Araújo, G. R. Oliveira, N. S. Fernandes, C. L. P. S. Zanta, S. S. L. Castro, D. R. Da Silva and C. A. Martínez-Huitle, *Environ. Sci. Pollut. Res.*, 2014, **21**, 9777–9784.

18 C. M. Schroeder, A. León Sandoval, K. K. Ohlhorst and N. E. Leadbeater, *Chem.: Methods*, 2023, **3**, e202300014.

19 C. M. Schroeder, T. M. Koehler, K. K. Ohlhorst and N. E. Leadbeater, *RSC Adv.*, 2023, **13**, 33559–33565.

20 C. M. Schroeder, T. M. Koehler and N. E. Leadbeater, *RSC Adv.*, 2024, **14**, 38385–38390.

21 G. Kuchtová, P. Mikulášek and L. Dušek, *Monatsh. Chem.*, 2022, **153**, 237–243.

22 A. B. De Souza, J. Mielcke, I. Ali, R. Dewil, T. Van De Goor and D. Cabooter, *J. Environ. Chem. Eng.*, 2023, **11**, 109993.

23 D. Zhi, Y. Lin, L. Jiang, Y. Zhou, A. Huang, J. Yang and L. Luo, *J. Environ. Manage.*, 2020, **260**, 110125.

24 L. D. Ardila-Leal, R. A. Poutou-Piñales, A. M. Pedroza-Rodríguez and B. E. Quevedo-Hidalgo, *Molecules*, 2021, **26**, 3813.

25 A. Iqbal, A. Yusaf, M. Usman, T. Hussain Bokhari and A. Mansha, *Int. J. Environ. Anal. Chem.*, 2023, 1–35.

26 S. Nakagawa, K. Sakakibara and H. Gotoh, *Dyes Pigm.*, 2016, **124**, 130–132.

27 S. Singh, V. C. Srivastava and I. D. Mall, *J. Phys. Chem. C*, 2013, **117**, 15229–15240.